

## Article

# Fatigue and Fracture Behaviors of Short Carbon Fiber Reinforced Squeeze Cast AZ91 at 20 °C and 250 °C

Nashmi H. Alrasheedi <sup>1</sup>, Mohamed M. El-Sayed Seleman <sup>2</sup> , Mohamed M. Z. Ahmed <sup>3,\*</sup>  and Sabbah Ataya <sup>1,\*</sup> 

<sup>1</sup> Department of Mechanical Engineering, College of Engineering, Imam Mohammad Ibn Saud Islamic University, Riyadh 11432, Saudi Arabia; nhrasheedi@imamu.edu.sa

<sup>2</sup> Department of Metallurgical and Materials Engineering, Faculty of Petroleum and Mining Engineering, Suez University, Suez 43512, Egypt; mohamed.elnagar@suezuniv.edu.eg

<sup>3</sup> Mechanical Engineering Department, College of Engineering at Al Kharj, Prince Sattam bin Abdulaziz University, Al Kharj 11942, Saudi Arabia

\* Correspondence: moh.ahmed@psau.edu.sa (M.M.Z.A.); smataya@imamu.edu.sa (S.A.)

**Abstract:** AZ91 is one of the most broadly used Mg alloys because of its good castability and reasonable mechanical properties. Strengthening AZ91 with carbon short fibers aims to increase tensile and fatigue strength, creep, and wear resistance. One of the proposed applications of reinforced AZ91 is the production of pistons for trucks. Such reciprocating parts are subjected to alternating fatigue loads which can lead to fatigue failure. In this respect, studying the tensile and fatigue behavior of materials subjected to such loading conditions is of great interest. The alternating low-cycle fatigue (LCF) and high-cycle fatigue (HCF) of unreinforced AZ91 and carbon fiber-reinforced AZ91 (AZ91-C) were investigated at 20 °C and 250 °C. Tensile tests were carried out at the same testing temperature to find the appropriate fatigue testing stress and strain for stress-controlled and strain-controlled tests, respectively. The fatigue curves of stress against the number of cycles (S–N) revealed that the composite AZ91-C's fatigue strength was 55 MPa under HCF, while that of the matrix alloy AZ91 was only 37 MPa at 250 °C. Fracture investigations were conducted on the broken test samples. The fracture approach in the matrix material (AZ91) is mixed ductile/brittle containing fatigue serration, fiber fracture, and separation in the reinforced material (AZ91-C).

**Keywords:** AZ91; composites; carbon short fibers; tensile strength; fatigue life; LCF; HCF



**Citation:** Alrasheedi, N.H.; El-Sayed Seleman, M.M.; Ahmed, M.M.Z.; Ataya, S. Fatigue and Fracture Behaviors of Short Carbon Fiber Reinforced Squeeze Cast AZ91 at 20 °C and 250 °C. *Crystals* **2023**, *13*, 1469. <https://doi.org/10.3390/cryst13101469>

Academic Editors: Wangzhong Mu and Chao Chen

Received: 19 September 2023

Revised: 2 October 2023

Accepted: 6 October 2023

Published: 9 October 2023



**Copyright:** © 2023 by the authors. Licensee MDPI, Basel, Switzerland. This article is an open access article distributed under the terms and conditions of the Creative Commons Attribution (CC BY) license (<https://creativecommons.org/licenses/by/4.0/>).

## 1. Introduction

The rapid development of technology today demands an increase in the quality of the products made. This is not only focused on attractive design but also on how the weight of the product can be reduced, thus leading to economic benefits and so on. For example, in the automotive and transportation sectors, weight reduction in parts or components leads to considerable fuel savings and environmental protection by lowering CO<sub>2</sub> emissions [1]. Over several decades, the production of parts in the automotive industry has been dominated by high-strength steels and aluminum alloys, but recently the application of magnesium alloys has received a lot of attention from practitioners and engineers worldwide [2]. It has been generally known that magnesium in its pure form is the most plentiful metal but has low mechanical properties, making its use in structural applications unlikely [3]. Different magnesium alloys can aid weight reduction more significantly than existing steels and aluminum, owing to their low density [4]. In addition, they have outstanding specific strength (strength to density ratio), favorable machinability, castability [5,6], damping capacity, and dimensional stability [7], which are advantages. In contrast to their advantages, magnesium alloys have a relatively low modulus of elasticity [8], poor corrosion resistance due to magnesium's high reactivity [9], and low mechanical strength and wear resistance, thus making them limited in scope for use in structural and friction-resistant applications [10].

The good castability of magnesium alloys makes them much more suitable for manufacturing complex parts with high precision, thus reducing machining costs, which should be seriously considered. Accordingly, some varieties of magnesium alloys have been extensively employed by automotive manufacturers [11]. Although the efforts to improve the properties and strength of the AZ91 alloy have been vigorous, the outcomes are still far from satisfactory. Therefore, it is imperative to conduct intensive research to attain better mechanical properties for the AZ91 alloy, especially the elastic modulus, creep resistance [12,13], and fatigue strength [14,15]. Furthermore, automotive components or parts in particular are subjected to periodic cyclic loading, which induces their failure during service [16,17]. This means that the fatigue properties of AZ91 alloys also need more attention to meet the criteria that are necessary in the rapidly growing automotive industry. There have been several experiments conducted to analyze the fatigue behavior of the AZ91 alloy [18,19], either at low-cycle fatigue or high-cycle fatigue, but there is still a need to upgrade it accordingly to enable products made from magnesium alloys that are truly suitable for future use. Rettberg et al. [20] performed reasonable investigations of the low-cycle fatigue behavior of AM60 and AZ91 alloys. The results showed that AM60 had higher ductility and, hence, a higher increase in fatigue life than AZ91 at higher strain amplitudes. At the lowest strain of 0.2 percent, AZ91 was more susceptible to pore position and size initiation than AM60, ultimately impacting its fatigue life. The fatigue behavior of the as-cast AZ91 alloy was reported in [21,22], where the S–N curve results revealed that the region with a high number of cycles to failure was still relatively low, and the fatigue limit range was between 60 and 85 MPa. Meanwhile, the effect of the ECAP process on the fatigue behavior of the AZ91 alloy was investigated [23], and it was found that the effect of the ECAP was not so evident, where the amplitude stresses of the AZ91 alloy as-cast and the AZ91 alloy as-ECAP were 80 MPa and 85 MPa, respectively, at an endurance limit based on  $10^7$  cycles. That means that in the high-cycle fatigue range there is not much of an effect, even though the AZ91 alloy has been subjected to the ECAP process. In contrast, in the low-cycle fatigue region, the fatigue life considerably increases. By reviewing the existing results, it was determined that the fatigue behavior of the AZ91 alloy needs to be increased for future improvements since it is still relatively low.

An approach that has been undertaken as a solution for improving fatigue behavior is to transform the form of the magnesium materials from alloys to composites. Previous studies have reported that the incorporation of reinforcement materials has significantly improved the characteristics of reinforced Mg materials, involving mechanical strength [24], tribological behavior [25], and the modulus of elasticity [26,27]. Among the reinforcement materials that have been incorporated into the AZ91 magnesium alloy are carbon fibers [12], carbon nanotubes [28], alumina [29], tungsten disulfides [30], metal carbides SiC [31,32], and titanium diboride [33]. In terms of the fatigue behavior of magnesium composites, the incorporation of SiCp has been proven to improve their fatigue performance when compared to monolithic AZ91D [34]. Regarding AZ91 composites reinforced with short alumina fibers, it has been stated [35] that reinforcing the AZ91 alloy with a 0.25 volume fraction is effective in increasing its fatigue strength up to 85%. This increment can be understood as a better fatigue crack initiation resistance for the AZ91 composite as compared to the AZ91 alloy. A previous study addressing the LCF and HCF characteristics of a 23 vol% carbon fiber-reinforced AE42 Mg alloy identified that there was a two-fold increase in fatigue strength once its fatigue life reached  $10^7$  cycles at 250 °C, from initially 25 MPa to 52.7 MPa [17]. This result motivates the study of reinforced AZ91-C under fatigue loading.

In the present study, a short carbon fiber-reinforced AZ91 alloy was used since it has been found that incorporating short carbon fibers is an appropriate method for improving the hardness, strength, and wear characteristics of the matrix alloy AZ91 [36,37]. In addition, based on the results in the literature, there is still a research deficiency specifically on the behavior of the short carbon fiber-reinforced AZ91 alloy under cyclic loading, making it crucial and engaging for further investigation. Therefore, the goal of this research is to

evaluate the behavior of the reinforced AZ91 alloy with highly fractionated short carbon fibers both under low-cyclic fatigue and high-cyclic fatigue at different temperatures.

## 2. Experimental Details

The main materials used were an AZ91 magnesium alloy and its composites. The reinforcing material used was a short carbon fiber with a high volume fraction. The specifications of the carbon fibers used in this study were approximately 100  $\mu\text{m}$  in length with a diameter of approximately 7  $\mu\text{m}$  and a volume fraction ( $v_f$ ) of 0.23, which were quasi-isotropically dispersed within the AZ91 alloy matrix. The detailed chemical composition of the AZ91 alloy was Mg-9.05 Al, 0.88 Zn, 0.05 Si, 0.28 Mn, 0.001 Ni, and 0.004 Fe (wt%).

The matrix alloy and the carbon fiber-reinforced composite were produced using the squeeze casting process. A preform of short carbon fibers was prepared and preheated to 400  $^{\circ}\text{C}$ , and the matrix was superheated up to 730  $^{\circ}\text{C}$  to ensure well filling and fiber/matrix wetting upon squeezing the melt into the preform. The materials were cast into truck pistons and samples were machined from these piston blocks. A more detailed description of the production, characterization, and evaluation of these materials is reported in [1,2]. Figure 1 shows a graphical flow chart containing the main preparation and testing steps. The test samples were machined to be loaded in parallel to the strengthened plane. In the current study, fatigue testing was conducted at three different temperatures, namely 20, 150, and 250  $^{\circ}\text{C}$ , on the unreinforced and reinforced magnesium alloy AZ91.

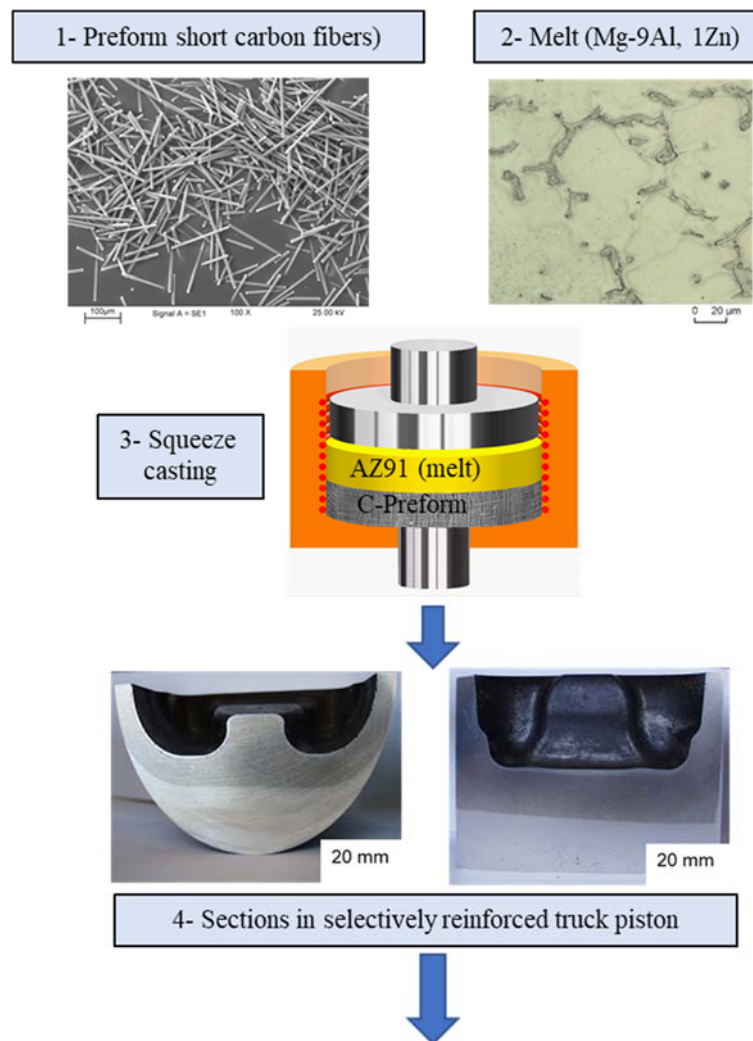
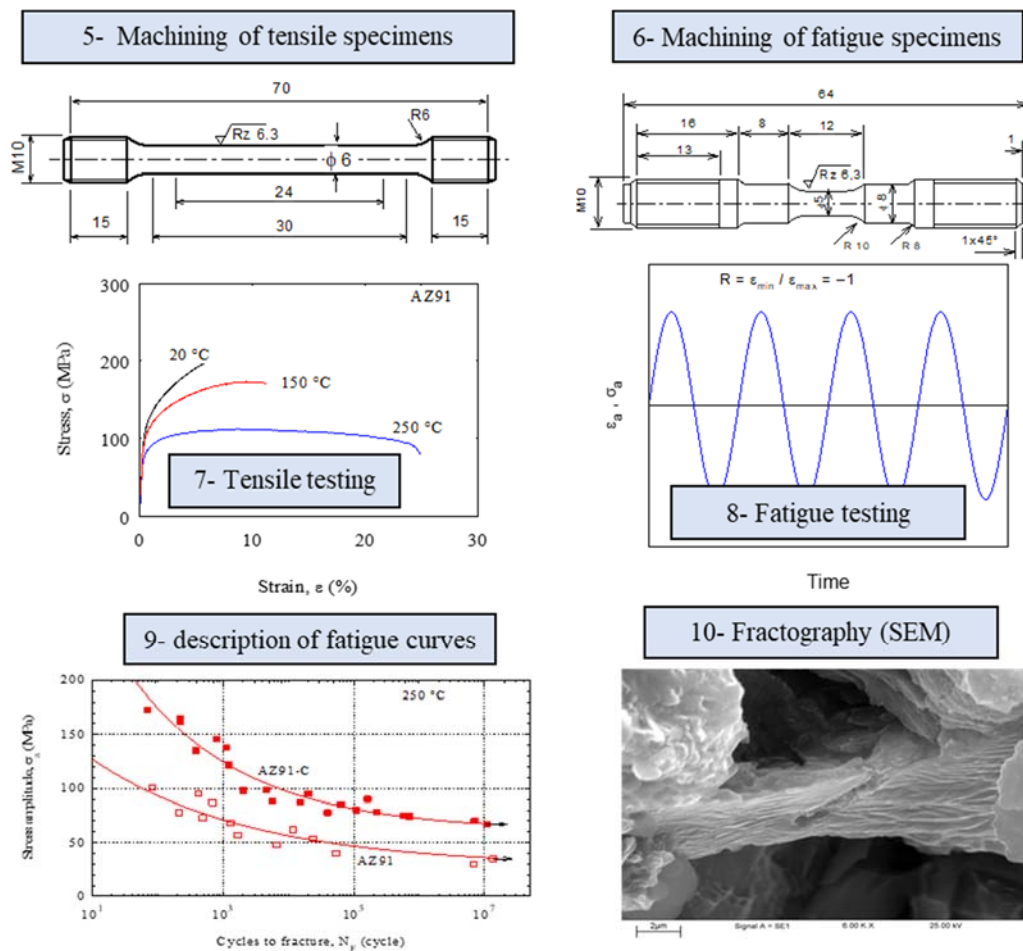


Figure 1. Cont.



**Figure 1.** Flow chart with images showing the main sequence for conducting the investigation method.

The microstructures of the cast matrix alloy AZ91 and the composite AZ91-C were investigated using optical microscopy. Samples were molded for classical mechanical grinding and polishing. The polished specimens were prepared for optical microscopy by etching with 2% Nital and applying an etching time of 15 s. The light microscope Leica DM4000M (Leica Microsystems GmbH, Wetzlar, Germany) was used. The hardness of the studied materials was measured using a low-load Vickers hardness tester of Type HWDV-7S (TTS Unlimited, Osaka, Japan) with a load of 2 N for a dwell time of 15 s. An average Vickers hardness value of 10 indentations was calculated.

Samples of both tensile and alternating fatigue ( $R = -1$ ) were examined in this study. Specifically, the tensile samples were prepared in a standard small-size sample according to ASTM E8 [24], while the fatigue samples were prepared following the ASTM E466 standard [25,26]. Two tensile test samples were tested for each temperature. The quasi-static tensile and cyclic tests were performed using a universal servo-hydraulic testing machine of MTS 810 (MTS Systems Corporation, Eden Prairie, MN, USA). The machine had a maximum capacity of 100 kN and a high rate of displacement of 100 mm/sec. This machine was fitted with a heating furnace that could be heated up to an upper temperature of 800 °C. Room temperature strain was measured with an extensometer that had an accuracy of 0.5  $\mu$ m and a maximum displacement of 10 mm. For high-temperature testing, the extensometer used had the following criteria: it was equipped with an inductive rod and had a sensitivity of 1  $\mu$ m and an upper displacement of 40 mm. The utilization of this extensometer was set at the strain-controlled LCF interval. The fatigue tests were performed at a frequency of 0.5 Hz with alternating strain control in the LCF interval of

$N < 10^4$  cycles, while the HCF interval was  $N > 10^4$  cycles. Concurrently, stress-controlled examinations were carried out at a frequency and load cycles of 50 Hz and  $2 \times 10^7$ , respectively. The applied ratio of alternating strain and stress in all tests was  $R = -1$  (minimum stress/maximum stress). The fatigue tests were performed until the sample was broken or stopped after exceeding a fatigue limit of  $10^7$  cycles. To construct the S–N curves, 16 to 17 test samples were used at the different stresses. Fracture investigation was carried out using a LEO Type 1450VP scanning electron microscope (SEM) with a voltage of 30 kV, fitted with an Oxford Type EDS detector to determine their composition. The sequence of the actions carried out in the study are systematically summarized as shown in Figure 1.

### 3. Results and Discussion

#### 3.1. Microstructure and Hardness Measurement Results

AZ91 possesses some advantages in comparison to other types of magnesium alloys, such as high strength, outstanding castability, and being notably less expensive. In contrast, at temperatures greater than 140 °C, the creep resistance of AZ91 is poor [12]. This alloy has been selected for application in the manufacture of pistons made of composite materials after being reinforced with carbon fiber to improve strength and creep resistance. Figure 2 includes the casting microstructure structure of AZ91 and the reinforced AZ91-C. The cast microstructure of the matrix alloy (Figure 2a) shows a massive dendrite structure, which is observable primarily along the grain boundaries, especially at the grains' triple points. The quantitative grain size measurement indicates that the average grain size is  $53 \pm 11 \mu\text{m}$ . The grain boundaries, containing mainly a  $\beta$ -phase of  $\text{Mg}_{17}(\text{Al})_{12}$  and  $\text{MgZn}$  and the grain matrix, are composed of an  $\alpha$ -Mg phase which contains the rest of the alloying Al additive mixed with magnesium [38,39]. A large overview of the composite material (AZ91-C) microstructure is presented in the as-polished section shown in Figure 2b. The fibers are randomly distributed in the matrix material and the fiber length is mostly laying on the reinforced plan. Figure 2c shows an optical image of etched samples, where no grain boundaries were revealed. This could be related to the presence of the high volume fraction of the fibers ( $V_f = 0.23$ ) which act as nucleating agents, giving no chance to build the segregated structure at the grain boundaries. Some dispersed precipitates of intermetallic compounds are revealed in the matrix area and others can be seen at the fiber/matrix interface.

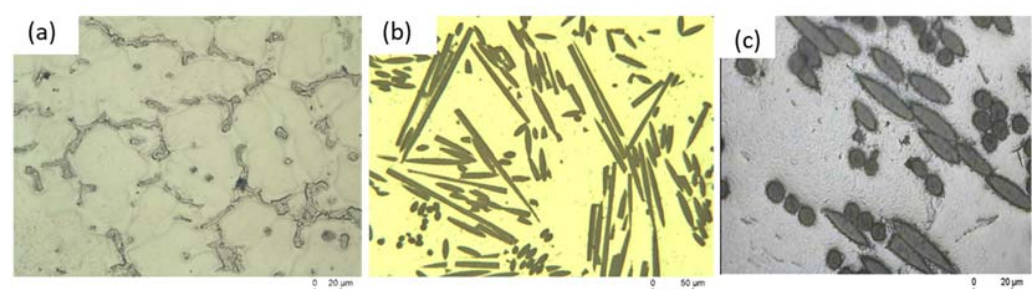


**Figure 2.** Microstructure of the investigated materials; (a) matrix (AZ91) [39] and (b) overview of polished composite (AZ91-C) [39] and (c) higher magnification for etched composite.

From the results obtained for the hardness test, the hardness of the unreinforced AZ91 was  $69.2 \pm 2 \text{ Hv}$ , while the hardness of the reinforced AZ91-C was  $111.53 \pm 4 \text{ Hv}$ . A remarkable increase in the hardness value of the unreinforced AZ91 of about 61.17% was found, owing to the influence of the short carbon fiber. Simultaneously, this proves that carbon fibers are efficient for becoming a potential type of reinforcement. In addition, these results are comparable to those obtained by other researchers [40,41]. It is worth mentioning that the applied hardness tester is a Vickers macro-hardness tester, and the diagonal of indentation ranged between 0.28 and 0.30 mm for the composites. The fiber diameter was about 7  $\mu\text{m}$ . It means that the indentation diagonal of the composites is approximately

equal to 40 times the fiber's diameter. In other words, the hardness measurements of the composite material are reliable.

### 3.2. Results of the Tensile Test

Figure 3 exhibits the stress–strain diagram of both unreinforced (AZ91) and reinforced (AZ91-C) at temperatures varying from room temperature to 300 °C. Both AZ91 and AZ91-C reveal a rapid increase in the flow stress during the initial stage of the deformation process, as shown in Figure 3. This is identified by the increase in the flow stress from 200 MPa for the unreinforced AZ91 to 265 MPa for the reinforced AZ91, which is clearly seen with a percentage of about 32.5% at 20 °C; this is the maximum stress achieved by both materials. This increase in stress experienced in the reinforced AZ91 can be directly understood as due to the addition of carbon fiber in the appropriate amount so that the carbon fiber can function properly [42]. In addition, the observed enhancement can be related to the onset of work hardening within the AZ91 alloy acting as the matrix, where the accumulation of continuous dislocations and kinks can promote the increase in strength of the reinforced AZ91 [43]. Another reason is the possibility of carbon fiber distribution occurring at the grain boundaries in the AZ91 alloy matrix, where grain growth is inhibited, allowing for the increased tensile stress of the reinforced AZ91 [44].

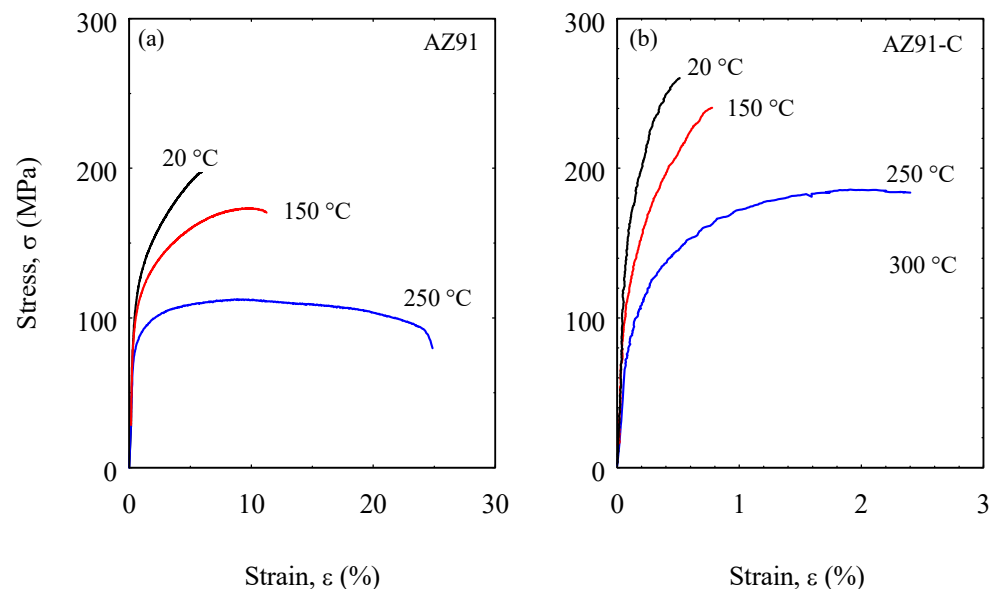


**Figure 3.** Comparison of stress–strain diagram of (a) unreinforced AZ91 and (b) reinforced AZ91-C at temperatures up to 300 °C.

Taking a further look, it is apparent that the tensile strength of both types of materials clearly decreases with increasing testing temperature (Figure 3). However, in general, the tensile strength of AZ91-C remains clearly higher than that of the unreinforced AZ91 at all temperatures. This means that an increase in temperature can cause a softening effect in both types of materials where dislocation rearrangement occurs, and concurrently, there is also a progressive dismantlement of the dislocations [45]. The uniqueness of the tensile test results seen in Figure 3 lies in the combination of opposing interactions in the tensile strength behavior of both materials, namely work hardening and dynamic softening. This indicates that temperature is an important factor that needs to be seriously considered in the strengthening mechanisms of materials. Even though the incorporation of short carbon fibers demonstrated the ability to enhance the tensile strength of reinforced AZ91 in general, there is a noticeable side effect in that the reinforced AZ91-C appeared to be more brittle and, thus, easily fractured during testing. This relates to its lower strain or ductility values if compared with the unreinforced AZ91 alloy. The short carbon fiber-reinforced AZ91 resulted in more limited plastic deformation at various temperatures.

Figure 4 compares the results of tensile yield stress ( $\sigma_{0.2}$ ), ultimate tensile stress ( $\sigma_{UTS}$ ), and strain ( $\epsilon$ ) between the matrix alloy AZ91 and the composite material AZ91-C at varying temperatures. The results presented are the average of the two tests, and the standard error has been calculated and presented in Figure 4. Table 1 includes the average values of the yield stress and the ultimate tensile strength for both the matrix alloy (AZ91) and the composite material (AZ91-C) as well as the improvement (in percent) that occurred at the different test temperatures. There is a noticeable improvement in the yield stress when reinforcing with carbon fibers. A downward trend is evident in the yield stress and the ultimate stress for both types of materials, but the reduction level in reinforced AZ91-C is somewhat greater than that of unreinforced AZ91 with increasing temperature. A high improvement in yield stress was attained at room temperature ( $\approx 108\%$ ). With an increase in the test temperature, the increase in the yield stress changed to 73% and 64% at 150 °C and 250 °C, respectively. A lower improvement in the ultimate tensile strength was noticed, where the increase in strength ranged between 30% and 64%.

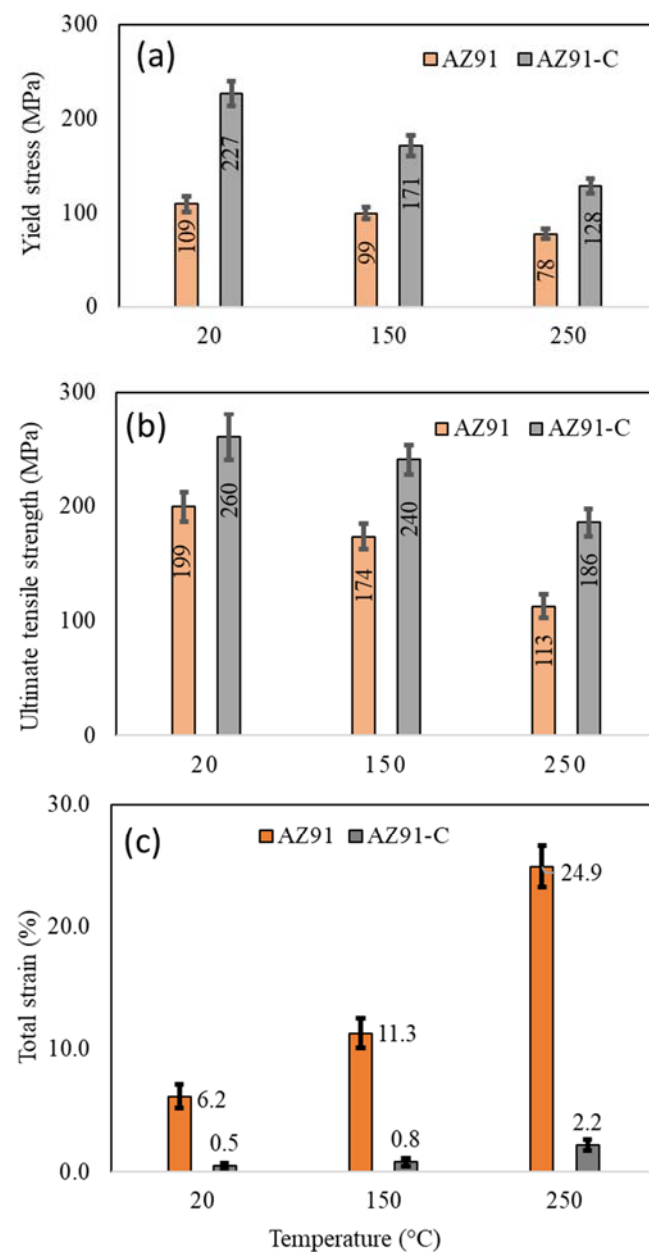


**Figure 4.** Tensile yield stress ( $\sigma_{0.2}$ ) (a), ultimate tensile strength ( $\sigma_{UTS}$ ) (b), and strain of the unreinforced AZ91 and reinforced AZ91-C (c) at temperatures 20, 150, and 250 °C.

**Table 1.** Improvement in tensile yield stress and ultimate tensile strength of AZ91 due to carbon short fiber reinforcement at different test temperatures.

Temperature	Yield Stress			Ultimate Tensile Strength		
	AZ91 (MPa)	AZ91-C (MPa)	Increase (%)	AZ91 (MPa)	AZ91-C (MPa)	Increase (%)
20 °C	109	227	107.89	199	260	30.61
150 °C	99	171	72.21	174	240	38.58
250 °C	78	128	65.16	113	186	64.92

The variation in yield strength improvement with temperature can be explained in light of the limited deformation range up to the yield stress of the composite. Moreover, the carbon fibers can be considered rigid bodies, where the strain of the carbon fibers up to fracture is very small (1.2–1.5%) [39]. At this deformation region, the contribution of the realignment of the fibers to carrying the applied load is very limited. There are two components that share the carrying of the applied stress: the matrix alloy (AZ91) which is greatly affected by the temperature and the rigid fibers which are unaffected by the temperature. Hence, the effect of temperature in the matrix material dominates the entire behavior of the composite materials. With the development of the deformation process, the fibers align with the applied load and contribute with the matrix in the deformation process, thus showing an improvement with temperature opposite to what has been obtained in the improvement of the yield stress.

The strengthening effect due to work hardening is more influential at low temperatures, while at higher temperatures it promotes softening due to dynamic recrystallization [46]. Regarding strain, the percentage strain of unreinforced AZ91 is greater than that of reinforced AZ91-C. This confirms that the unreinforced AZ91 has great ductility, while the reinforced AZ91-C is more brittle. However, one thing that needs to be highlighted is that the ductility of both materials increases with increasing temperature. Even with a general decrease in the materials' strength given an increase in the test temperature, the percent improvement in the composite's ultimate tensile strength increases with the increasing temperature. This indicates that the thermal stability of the reinforced materials (AZ91-C) is much higher than that of the matrix AZ91 alloy. The increase in the percent improvement of the ultimate tensile strength encourages the application of this composite material for high-temperature uses. Of equal importance, the key values obtained from the tensile test can be used as guidelines in the determination of the initial fatigue stress amplitude, which should be slightly higher than the yield stress.

### 3.3. Fatigue Testing Results

The fatigue (S–N) curves, as shown in Figure 5, are plotted based on the empirical arbitrary exponential formula [17] as described in Equation (1):

$$\sigma_a = a \frac{\exp(-\log N)}{b^2} + c. \quad (1)$$

where  $\sigma_a$  is the stress amplitude, N is the number of cycles, a, b, and c are constants.

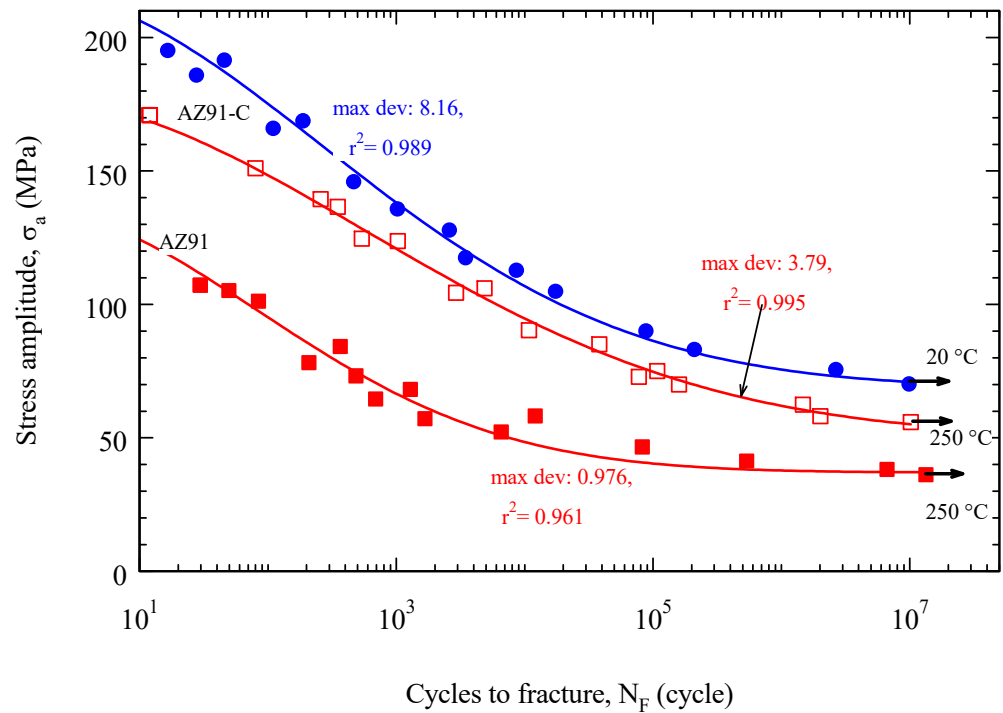


**Figure 5.** Fatigue S–N curves of AZ91-C and AZ91 at different temperatures.

Table 2 presents the constants obtained by fitting the fatigue curves at varying temperatures. The fatigue strength is calculated by the description of the curve as the fatigue stress at the attainable life ( $N = 10^7$  cycles). For further details, the fatigue strength and the value of the different fitting parameters are given in Table 2.

**Table 2.** The fitting parameters of the S–N fatigue curves of unreinforced AZ91 and AZ91-C together with their fatigue strengths at  $N = 10^7$  cycles.

Specimen	No. of Experiments	T (°C)	a	b	c	Max. Dev.	Standard Error, $r^2$	Fatigue Strength (MPa) at $N = 10^7$
AZ91	16	250	100	2.72	37	0.976	0.961	37
AZ91-C	16	20	150	3.42	68.7	8.16	0.989	71.2
	17	250	128	3.90	50	3.79	0.995	55

The S–N fatigue curve fitting parameters at the test conditions are listed in Table 2. The fatigue strength can be estimated from the curve fitting as the fatigue stress at the highest attained fatigue life ( $N = 10^7$  cycles). In addition, the fatigue resistance information is also provided in Table 2. The effect of reinforcement on fatigue strength can be judged at 250 °C. A percentage improvement in fatigue strength of about 92% was attained at 250 °C at the fatigue testing limit (at  $N = 10^7$  cycles). As the aimed application of this material is at high temperatures, such as pistons for trucks, the reinforced material was tested at both room temperature and at 250 °C to evaluate the stability of this material at high temperatures. Even though the fatigue strength values in both the AZ91 reinforced and unreinforced alloys are low, the results obtained are still better than those experienced by the AE42 alloy and its composites [17]. There is an interesting phenomenon in the results obtained with the magnesium alloy composite (AZ91-C) in the present study, if compared with other aluminum alloys as reported in [47], where the fatigue strength of the AA6061 alloy was 100 MPa at room temperature and  $10^7$  cycles. Moreover, the fatigue strength of the AE42 alloy composite (AE42-C) was only 70.5 MPa under the same test conditions [17].

Figure 6 shows examples of the fatigue hysteresis loops at 250 °C under a strain amplitude of  $\varepsilon_a = 0.02$  for the matrix alloy AZ91 (Figure 6a) and the composite material AZ91-C (Figure 6b). Figure 6a shows the three individual hysteresis loops of the unreinforced alloy AZ91 at 250 °C under a strain amplitude of  $\varepsilon_a = 0.02$ . There is some material softening after several cycles of 670. Softening can be noticed when decreasing the attained stress at the applied strain amplitude due to the high testing temperature. Applying the same strain amplitude on the reinforced AZ91-C materials (Figure 6b) shows a higher stress level that is nearly double of that which appeared for the unreinforced AZ91. And the fracture takes place very fast, after only three cycles.

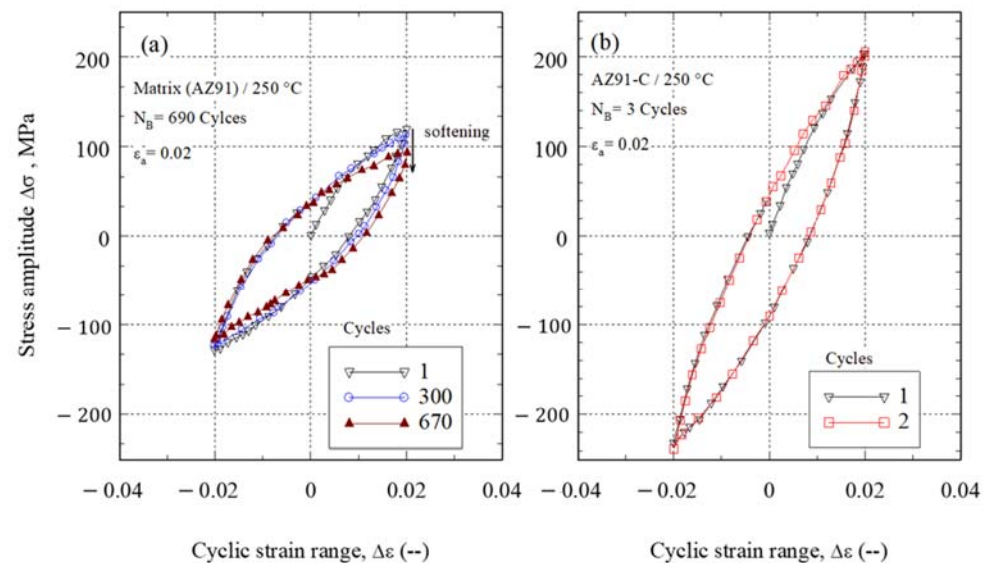


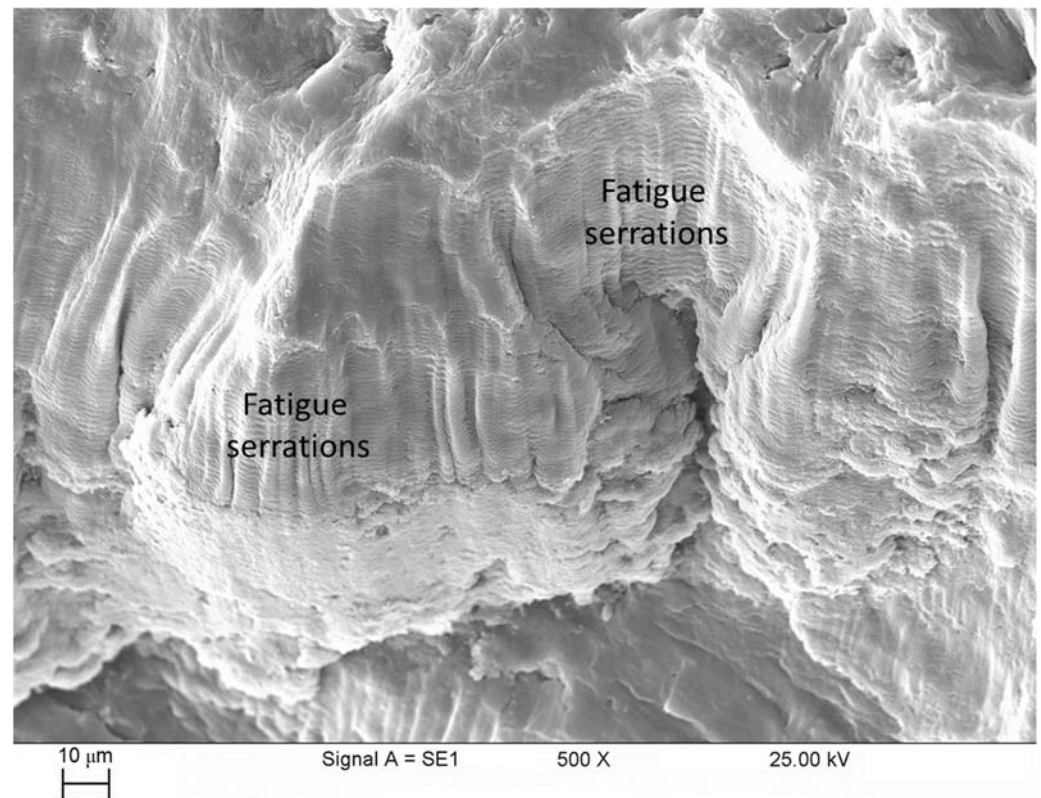
**Figure 6.** Hysteresis loops at 250 °C under strain amplitude of  $\varepsilon_a = 0.02$  for (a) the matrix alloy AZ91 (b) and the composite material AZ91-C.

Cyclic straining of AZ91 at 250 °C ( $0.56 T_m$ ) with a strain amplitude of  $\varepsilon_a = 0.02$  resulted in cyclic softening affected by material recrystallization at this high temperature. Similar cyclic softening accompanied with a decrease in life has been detected on LCF testing of cast AZ91 at temperatures higher than 200 °C [48]. Such behavior is noted to decrease the material's fatigue strength. Some of the reasons related to this softening are grain boundary sliding, formation of discontinuous precipitates, and softening of the  $\beta$ -Mg<sub>17</sub>Al<sub>12</sub> phase at elevated temperatures [48].

### 3.4. Fractography (SEM)

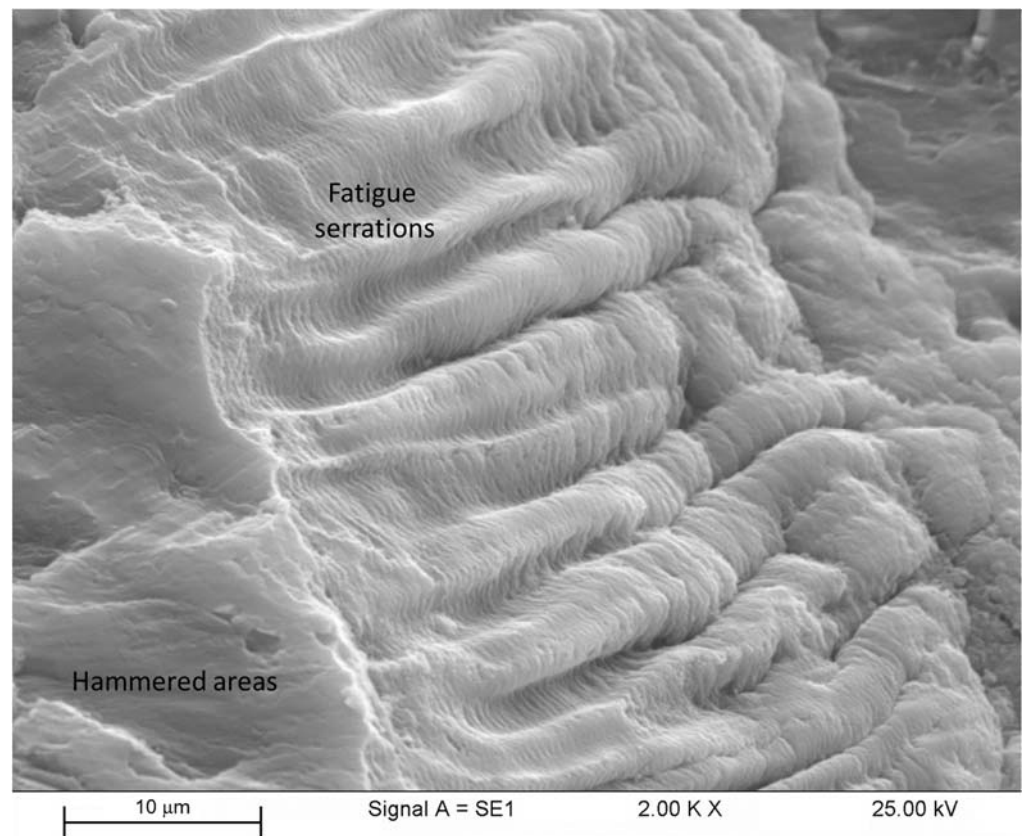
Figure 7 presents the fatigue fracture features of an unreinforced AZ91 fatigue specimen at a temperature of 250 °C, a stress amplitude of 41 MPa, and a fatigue life of  $5.4 \times 10^5$  cycles. By observing the fatigue fracture, it can be seen that the formation of fine serrations dominates almost all parts of the unreinforced AZ91 fatigue fracture surface in the HCF range and has a low stress amplitude of 41 MPa at 250 °C. The formation of fine serrations is caused by serration flow, which is closely related to dynamic strain aging (DSA). It has been explained by McCormick [49] that this dynamic strain aging occurs when the forest dislocation successfully restrains the movement of the dislocation, and finally, the solute atoms undergo diffusion towards the restrained dislocation. This phenomenon promotes an increase in the flow stress enhanced by the hindering factor of dislocation movement. Under some conditions, the restrained dislocation may release itself from the atmospheric environment of the solute when the flow stress successfully reaches its critical value. For this reason, a lower stress is required to evacuate the dislocation so that it returns to the following dislocation forest [49–51]. It was further found that the relationship between the serrated flow and the dynamic strain aging was induced by the factor of excess mag-

nesium [52,53]. This serrated flow could also result from the repeated dynamic effects of pinning and unpinning [54,55]. It is also suggested that the serrations are formed due to the competition between the precipitate displacement caused by the dislocations and the dynamic strain aging [50,55].



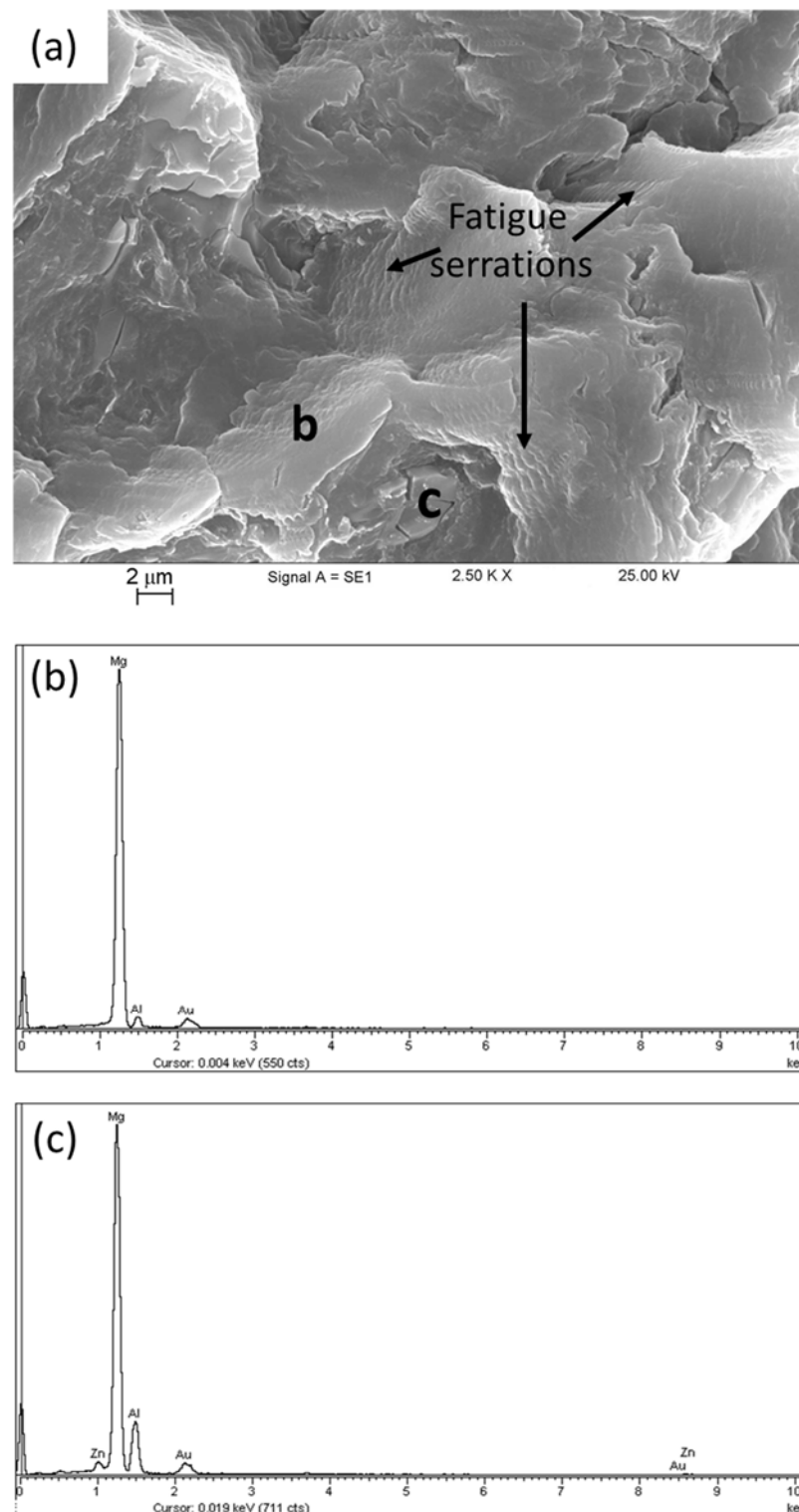
**Figure 7.** Fatigue fracture features of fractured fatigue specimen of the unreinforced AZ91 at 250 °C, stress amplitude of 41 MPa, and fatigue life of  $5.4 \times 10^5$  cycles.

Figure 8 exhibits the perspicuous fatigue serrations and flattened areas by hammering the mating surfaces on an unreinforced AZ91 fatigue fracture specimen at 250 °C with a stress amplitude of 41 MPa and a fatigue life of  $5.4 \times 10^5$  cycles. From the appearance of the fatigue fracture, two different contrast areas are evident. There is an area consisting of fatigue serrations that remain in their undamaged condition at the center, to the right of the fatigue fracture surface. On the other hand, there is also a small portion on the left side of the fatigue fracture surface that has evolved to be flattened due to the hammering of the opposite specimen's surface for the fatigue fracture surface in the unreinforced AZ91 [56]. If the flattened surface is further observed, cracks can be seen spanning the fatigue fracture's surface. The cracks cooperate with multiple grains on fatigue loading, producing a large reverse plastic zone. This eventually induces the synchronized creation of planar slip bands on multiple grains leading to a flattened crack [57].



**Figure 8.** Perspicuous fatigue serrations and flattened areas by hammering the mating surfaces on an unreinforced AZ91 fatigue fracture specimen at 250 °C, stress amplitude of 41 MPa, and fatigue life of  $5.4 \times 10^5$  cycles.

Figure 9 shows a magnified view of the unreinforced AZ91 fatigue specimen fracture surface at 250 °C, supplemented with EDS analysis of the ductile region with multiple dimples and cleavage surfaces containing cracks, indicating the brittle region. From the fatigue fracture surface, it is possible to distinguish ductile areas containing some dimples and brittle areas containing cleavages decorated with cracks. Crack initiation generally occurs in the softer region, referring to the ductile region, due to continuous cyclic loading. As a result, the fatigue fracture surface explicitly shows cracks propagating over the ductile fatigue serrations, which can be readily observed. Further examination of the ductile regions containing dimples (as indicated in point b) using EDS showed that the Mg concentration was very high, followed by the presence of Al in low concentrations. This means that the ductile region contains poor Zn and Zn compounds, which confirms that Zn-containing precipitates are not formed in the ductile region. In contrast, the EDS analysis of the brittle region (indicated by point c) clearly reveals that the highest peak is dominated by Mg, and there is an increase in Al concentration when compared to point B, but interestingly, Zn is identified in the brittle region. As is known, Zn and Mg have an equal valence electron number; this results in a very low concentration of electrons. Likewise, when viewed in terms of the atomic radius between Zn and Mg, where the atomic radius of Zn has a very close proximity to Mg, the presence of Zn can replace Mg atoms to encourage the occurrence of precipitated phases in the form of intermetallic compounds in brittle areas. The absence of Zn in the ductile region may refer to intermetallic  $Mg_{17}Al_{12}$  formation [58], while at the brittle zone the phases formed are  $\tau$ - $Mg_{32}(Al,Zn)_{49}$  and  $\phi$ - $Mg_5Al_2Zn_2$  [59], where it is affected by the presence of Zn and also Al in low concentrations. Additionally, the cracks that appeared in the brittle area are the result of material decohesion occurring in the Zn-rich intermetallic precipitate phases.



**Figure 9.** EDX spectrum of the unreinforced AZ91 fatigued specimen at 250 °C (a) Higher magnification, (b) EDX analysis spectrum of ductile regions with Zn-poor dimple, and (c) EDX spectrum on cleavage fracture with cracks at the Zn-containing region.

Figure 10 shows the features of the composite AZ91-C fatigue-fractured test sample at 20 °C. There is an observable phenomenon where the area consisting of fatigue serrations appears to be split due to cracks propagating in the perpendicular direction of the metal connection between the carbon fibers, so that the fatigue serrations appear to be separated,

as specified in Figure 10. In addition, the presence of considerable dimple features under the fatigue serrations indicates the presence of large plastic deformation in the reinforced AZ91 sample [60]. Carbon fiber breaks are also seen located adjacent to the dimples. This can be understood due to the brittle nature of carbon fiber, which indicates its inability to respond to the deformation of the matrix material.

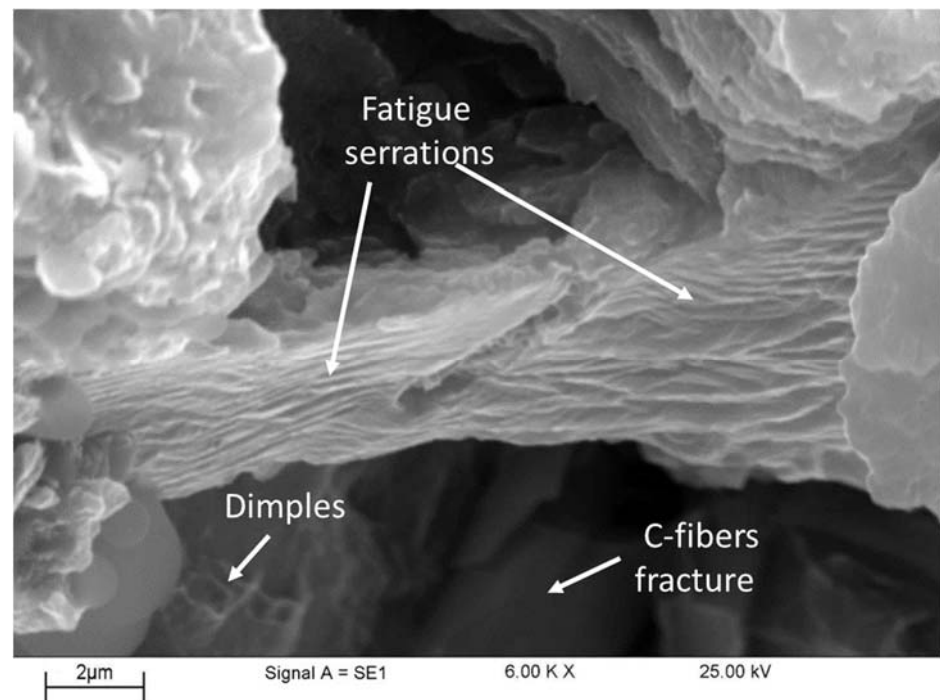


**Figure 10.** The features of the reinforced AZ91 fatigue fracture specimen at room temperature.

Figure 11 shows the features of the reinforced AZ91 fatigue-fractured specimen at 150 °C. The beginning state of carbon fiber is that it is encased in a metallic material that acts as a matrix bridge. However, being under continuous vibration stress causes crack initiation, which undergoes crack growth and propagation at the metal joints between the carbon fibers, resulting in fatigue fracture [17]. Then, a fractured metal joint is indicated by the formation of dimple features at the separation of the ductile metallic junction of the matrix alloy. There is a phenomenon of carbon detachment from the alloy matrix that causes it to stand independently without any support. The brittle nature of carbon fiber leads to fracture due to its inherent lack of response to the deformation of the matrix alloy. Li et al. stated that metal matrix composites reinforced with continuous fibers usually fracture at relatively low stress conditions without any damage found on the fiber surface after the manufacturing process [61]. In metal matrix composites, the mechanical properties are not only influenced by the constituents but, more importantly, the conditions between the fiber and the matrix, known as the interface [62]. If the interface has low strength, cracks will initiate in the brittle fibers which are more likely to shift and debond the fibers, leading to a single fiber pull, which has the effect of reducing stress concentration [63]. In this study, the fact that interface debonding prevailed under low stress conditions, as well as the ability of carbon fibers to withstand load, was not completely followed by lower flexural strength. In contrast to composites with moderate levels of interfacial strength, when micro-cracks start on the brittle carbon fibers, they will propagate and then terminate at the interface, i.e., on carbon fibers or a ductile matrix. Nevertheless, the main characteristic of composites with moderate interfacial bond strength is the occurrence of broken fiber bonds [64].

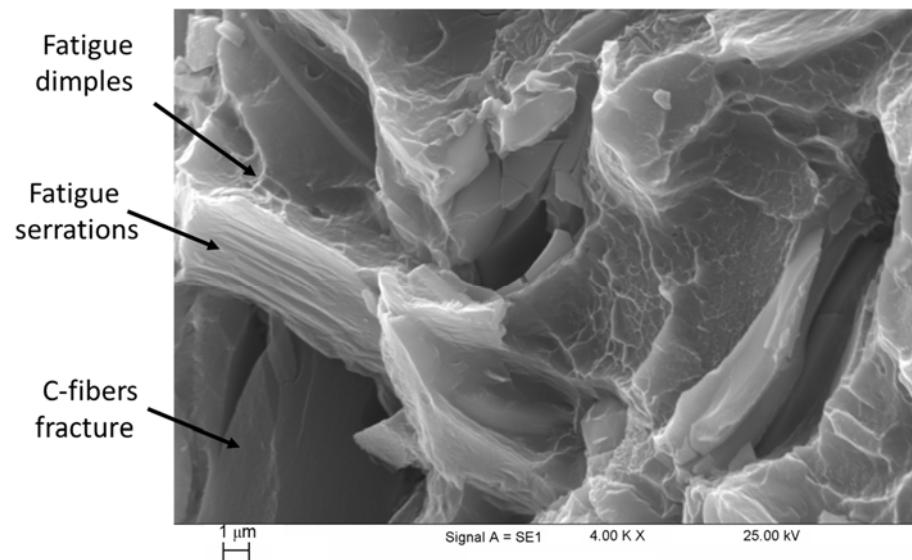


**Figure 11.** Fatigue fracture features of a fractured fatigue specimen of the reinforced AZ91 at 150 °C.

#### 4. Conclusions

From the mechanical characterization of the unreinforced and reinforced AZ91 using hardness and tensile testing as well as the fatigue tests conducted and the fractographic investigations, the following conclusions have been drawn:

- (1) The hardness value of the unreinforced AZ91 increased from  $69.2 \pm 2$  Hv to  $111.53 \pm 4$  Hv for the reinforced AZ91-C;
- (2) A clear improvement in yield stress was achieved at room temperature (108%); this improvement changed to 73% and 64% at 150 °C and 250 °C, respectively. A relatively lower improvement in the ultimate tensile strength was noticed, where the increase in strength ranged between 30% and 64%;
- (3) The fatigue strength at HCF range (over  $10^7$  cycles) at 250 °C for the AZ91 alloy was 37 MPa, while that for the reinforced AZ91-C reached 55 MPa. The reinforced AZ91-C displayed higher fatigue strength (71.2 MPa) at room temperature;
- (4) The hysteresis loops for the strain-controlled fatigue test of AZ91 at 250 °C showed limited material softening;
- (5) Diffused fatigue serrations with mixed ductile/brittle modes were observed on unreinforced AZ91's fracture surface;
- (6) Fiber fracture and fiber decohesion were noticed on the composite's fracture surface both under tensile and fatigue loads. The presence of fatigue serrations and regions exhibiting restricted dimples was detected in metallic magnesium zones.

**Author Contributions:** Conceptualization, N.H.A., S.A. and M.M.Z.A.; methodology, S.A. and M.M.E.-S.S.; validation, S.A. and M.M.E.-S.S.; formal analysis, S.A. and M.M.Z.A.; investigation, S.A. and M.M.Z.A.; resources, N.H.A.; writing—original draft preparation, N.H.A. and M.M.E.-S.S.; writing—review and editing, M.M.E.-S.S., M.M.Z.A. and S.A.; supervision, N.H.A., S.A. and M.M.Z.A.; project administration, N.H.A. and S.A.; funding acquisition, S.A. and N.H.A. All authors have read and agreed to the published version of the manuscript.

**Funding:** Funded by the Deanship of Scientific Research at Imam Mohammad Ibn Saud Islamic University, Saudi Arabia, through grant No. (221414016).

**Data Availability Statement:** Data are available upon request through the corresponding author.

**Acknowledgments:** The authors extend their appreciation to the Deanship of Scientific Research, Imam Mohammad Ibn Saud Islamic University (IMSIU), Saudi Arabia, for funding this research study through grant No. (221414016).

**Conflicts of Interest:** The authors declare no conflict of interest.

## References

1. Joost, W.J.; Krajewski, P.E. Towards Magnesium Alloys for High-Volume Automotive Applications. *Scr. Mater.* **2017**, *128*, 107–112. [\[CrossRef\]](#)
2. Demirci, E.; Yildiz, A.R. An Investigation of the Crash Performance of Magnesium, Aluminum and Advanced High Strength Steels and Different Cross-Sections for Vehicle Thin-Walled Energy Absorbers. *Mater. Test.* **2018**, *60*, 661–668. [\[CrossRef\]](#)
3. Kumar, D.S.; Sasanka, C.T.; Ravindra, K.; Suman, K.N.S. Magnesium and Its Alloys in Automotive Applications—A Review. *Am. J. Mater. Sci. Technol.* **2015**, *4*, 12–30. [\[CrossRef\]](#)
4. Kulekci, M.K. Magnesium and Its Alloys Applications in Automotive Industry. *Int. J. Adv. Manuf. Technol.* **2008**, *39*, 851–865. [\[CrossRef\]](#)
5. Tan, J.; Ramakrishna, S. Applications of Magnesium and Its Alloys: A Review. *Appl. Sci.* **2021**, *11*, 6861. [\[CrossRef\]](#)
6. Chalisgaonkar, R. Insight in Applications, Manufacturing and Corrosion Behaviour of Magnesium and Its Alloys—A Review. *Mater. Today Proc.* **2019**, *26*, 1060–1071. [\[CrossRef\]](#)
7. Ghaderi, S.H.; Mori, A.; Hokamoto, K. Analysis of Explosively Welded Aluminum-AZ31 Magnesium Alloy Joints. *Mater. Trans.* **2008**, *49*, 1142–1147. [\[CrossRef\]](#)
8. Cao, X.; Jahazi, M.; Immarigeon, J.P.; Wallace, W. A Review of Laser Welding Techniques for Magnesium Alloys. *J. Mater. Process. Technol.* **2006**, *171*, 188–204. [\[CrossRef\]](#)
9. Prasad, S.V.S.; Prasad, S.B.; Verma, K.; Mishra, R.K.; Kumar, V.; Singh, S. The Role and Significance of Magnesium in Modern Day Research-A Review. *J. Magnes. Alloy* **2022**, *10*, 1–61. [\[CrossRef\]](#)
10. Zhai, W.; Bai, L.; Zhou, R.; Fan, X.; Kang, G.; Liu, Y.; Zhou, K. Recent Progress on Wear-Resistant Materials: Designs, Properties, and Applications. *Adv. Sci.* **2021**, *8*, 2003739. [\[CrossRef\]](#)
11. Friedrich, H.; Schumann, S. Research for a “New Age of Magnesium” in the Automotive Industry. *J. Mater. Process. Technol.* **2001**, *117*, 276–281. [\[CrossRef\]](#)
12. Ataya, S.; El-Magd, E. Modeling the Creep Behavior of Mg Alloys with and without Short-Fiber Reinforcement. *Comput. Mater. Sci.* **2007**, *39*, 155–159. [\[CrossRef\]](#)
13. Srinivasan, A.; Ajithkumar, K.K.; Swaminathan, J.; Pillai, U.T.S.; Pai, B.C. Creep Behavior of AZ91 Magnesium Alloy. *Procedia Eng.* **2013**, *55*, 109–113. [\[CrossRef\]](#)
14. Lin, Y.C.; Chen, X.M.; Liu, Z.H.; Chen, J. Investigation of Uniaxial Low-Cycle Fatigue Failure Behavior of Hot-Rolled AZ91 Magnesium Alloy. *Int. J. Fatigue* **2013**, *48*, 122–132. [\[CrossRef\]](#)
15. Azadi, M.; Farrahi, G.H.; Winter, G.; Eichlseder, W. Fatigue Lifetime of AZ91 Magnesium Alloy Subjected to Cyclic Thermal and Mechanical Loadings. *Mater. Des.* **2014**, *53*, 639–644. [\[CrossRef\]](#)
16. Nascimento, L.; Yi, S.; Bohlen, J.; Fuskova, L.; Letzig, D.; Kainer, K.U. High Cycle Fatigue Behaviour of Magnesium Alloys. *Procedia Eng.* **2010**, *2*, 743–750. [\[CrossRef\]](#)
17. Alsaleh, N.A.; Ataya, S.; Latief, F.H.; Ahmed, M.M.Z.; Ataya, A.; Abdul-Latif, A. LCF and HCF of Short Carbon Fibers Reinforced AE42 Mg Alloy. *Materials* **2023**, *16*, 3686. [\[CrossRef\]](#)
18. Fintová, S.; Trško, L.; Chlup, Z.; Pastorek, F.; Kajánek, D.; Kunz, L. Fatigue Crack Initiation Change of Cast Az91 Magnesium Alloy from Low to Very High Cycle Fatigue Region. *Materials* **2021**, *14*, 6245. [\[CrossRef\]](#)
19. Chen, L.J.; Shen, J.; Wu, W.; Li, F.; Wang, Y.; Liu, Z. Low-Cycle Fatigue Behavior of Magnesium Alloy AZ91. *Mater. Sci. Forum* **2005**, *488–489*, 725–728. [\[CrossRef\]](#)
20. Rettberg, L.H.; Jordon, J.B.; Horstemeyer, M.F.; Jones, J.W. Low-Cycle Fatigue Behavior of Die-Cast Mg Alloys AZ91 and AM60. *Metall. Mater. Trans. A Phys. Metall. Mater. Sci.* **2012**, *43*, 2260–2274. [\[CrossRef\]](#)
21. Wolf, B.; Fleck, C.; Eifler, D. Characterization of the Fatigue Behaviour of the Magnesium Alloy AZ91D by Means of Mechanical Hysteresis and Temperature Measurements. *Int. J. Fatigue* **2004**, *26*, 1357–1363. [\[CrossRef\]](#)
22. Gu, X.N.; Zhou, W.R.; Zheng, Y.F.; Cheng, Y.; Wei, S.C.; Zhong, S.P.; Xi, T.F.; Chen, L.J. Corrosion Fatigue Behaviors of Two Biomedical Mg Alloys—AZ91D and WE43—In Simulated Body Fluid. *Acta Biomater.* **2010**, *6*, 4605–4613. [\[CrossRef\]](#) [\[PubMed\]](#)
23. Fintová, S.; Kunz, L. Fatigue Properties of Magnesium Alloy AZ91 Processed by Severe Plastic Deformation. *J. Mech. Behav. Biomed. Mater.* **2015**, *42*, 219–228. [\[CrossRef\]](#) [\[PubMed\]](#)
24. Ataya, S.; El-Magd, E. Quasi-Static Behavior of Mg-Alloys with and without Short-Fiber Reinforcement. *Theor. Appl. Fract. Mech.* **2007**, *47*, 102–112. [\[CrossRef\]](#)
25. Ataya, S.; Alsaleh, N.A.; El-Sayed Seleman, M.M. Strength and Wear Behavior of Mg Alloy AE42 Reinforced with Carbon Short Fibers. *Acta Metall. Sin. (English Lett.)* **2019**, *32*, 31–40. [\[CrossRef\]](#)
26. Aravindan, S.; Rao, P.V.; Ponappa, K. Evaluation of Physical and Mechanical Properties of AZ91D/SiC Composites by Two Step Stir Casting Process. *J. Magnes. Alloy* **2015**, *3*, 52–62. [\[CrossRef\]](#)
27. Lü, L.; Lai, M.O.; Gupta, M.; Chua, B.W.; Osman, A. Improvement of Microstructure and Mechanical Properties of AZ91/SiC Composite by Mechanical Alloying. *J. Mater. Sci.* **2000**, *35*, 5553–5561. [\[CrossRef\]](#)
28. Yuan, Q.H.; Zeng, X.S.; Liu, Y.; Luo, L.; Wu, J.B.; Wang, Y.C.; Zhou, G.H. Microstructure and Mechanical Properties of AZ91 Alloy Reinforced by Carbon Nanotubes Coated with MgO. *Carbon* **2016**, *96*, 843–855. [\[CrossRef\]](#)
29. Khandelwal, A.; Mani, K.; Srivastava, N.; Gupta, R.; Chaudhari, G.P. Mechanical Behavior of AZ<sub>31</sub>/Al<sub>2</sub>O<sub>3</sub> Magnesium Alloy Nanocomposites Prepared Using Ultrasound Assisted Stir Casting. *Compos. Part B Eng.* **2017**, *123*, 64–73. [\[CrossRef\]](#)

30. Huang, S.J.; Abbas, A. Effects of Tungsten Disulfide on Microstructure and Mechanical Properties of AZ91 Magnesium Alloy Manufactured by Stir Casting. *J. Alloys Compd.* **2020**, *817*, 153321. [[CrossRef](#)]
31. Wang, X.J.; Hu, X.S.; Wu, K.; Wang, L.Y.; Huang, Y.D. Evolutions of Microstructure and Mechanical Properties for SiCp/AZ91 Composites with Different Particle Contents during Extrusion. *Mater. Sci. Eng. A* **2015**, *636*, 138–147. [[CrossRef](#)]
32. Kumar, A.; Kumar, S.; Mukhopadhyay, N.K.; Yadav, A.; Sinha, D.K. Effect of TiC Reinforcement on Mechanical and Wear Properties of AZ91 Matrix Composites. *Int. J. Met.* **2022**, *16*, 2128–2143. [[CrossRef](#)]
33. Xiao, P.; Gao, Y.; Xu, F.; Yang, S.; Li, B.; Li, Y.; Huang, Z.; Zheng, Q. An Investigation on Grain Refinement Mechanism of TiB<sub>2</sub> Particulate Reinforced AZ91 Composites and Its Effect on Mechanical Properties. *J. Alloys Compd.* **2019**, *780*, 237–244. [[CrossRef](#)]
34. Vaidya, A.R.; Lewandowski, J.J. Effects of SiCp Size and Volume Fraction on the High Cycle Fatigue Behavior of AZ91D Magnesium Alloy Composites. *Mater. Sci. Eng. A* **1996**, *220*, 85–92. [[CrossRef](#)]
35. Llorca, N.; Bloyce, A.; Yue, T.M. Fatigue Behaviour of Short Alumina Fibre Reinforced AZ91 Magnesium Alloy Metal Matrix Composite. *Mater. Sci. Eng. A* **1991**, *135*, 247–252. [[CrossRef](#)]
36. Ataya, S.; El-Sayed Seleman, M.M.; Latief, F.H.; Ahmed, M.M.Z.; Hajlaoui, K.; Soliman, A.M.; Alsaleh, N.A.; Habba, M.I.A. Wear Characteristics of Mg Alloy AZ91 Reinforced with Oriented Short Carbon Fibers. *Materials* **2022**, *15*, 4841. [[CrossRef](#)]
37. Ataya, S.; El-Sayed Seleman, M.M.; Latief, F.H.; Ahmed, M.M.Z.; Hajlaoui, K.; Elshaghoul, Y.G.Y.; Habba, M.I.A. Microstructure and Mechanical Properties of AZ91 Rein-Forced with High Volume Fraction of Oriented Short Carbon Fibers. *Materials* **2022**, *15*, 4818. [[CrossRef](#)]
38. Shastri, H.; Mondal, A.K.; Dutta, K.; Dieringa, H.; Kumar, S. Microstructural Correlation with Tensile and Creep Properties of AZ91 Alloy in Three Casting Techniques. *J. Manuf. Process.* **2020**, *57*, 566–573. [[CrossRef](#)]
39. Alrasheedi, N.H.; Ataya, S.; El-Sayed Seleman, M.M.; Ahmed, M.M.Z. Tensile Deformation and Fracture of Unreinforced AZ91 and Reinforced AZ91-C at Temperatures up to 300 °C. *Materials* **2023**, *16*, 4785. [[CrossRef](#)]
40. Chen, B.; Fu, J.; Zhou, J.; Ma, Y.; Qi, L. Influence of Microstructures on Mechanical Properties of the Csf/Mg Composite Fabricated by Liquid-Solid Extrusion Following Vacuum Pressure Infiltration. *J. Alloys Compd.* **2023**, *935*, 168083. [[CrossRef](#)]
41. Hou, L.G.; Wu, R.Z.; Wang, X.D.; Zhang, J.H.; Zhang, M.L.; Dong, A.P.; Sun, B.D. Microstructure, Mechanical Properties and Thermal Conductivity of the Short Carbon Fiber Reinforced Magnesium Matrix Composites. *J. Alloys Compd.* **2017**, *695*, 2820–2826. [[CrossRef](#)]
42. Xu, H.; Yang, Z.; Hu, M.; Ji, Z. Effect of Short Carbon Fiber Content on SCFs/AZ31 Composite Microstructure and Mechanical Properties. *Results Phys.* **2020**, *17*, 103074. [[CrossRef](#)]
43. Wang, M.; Jin, P.; Wang, J. Hot Deformation and Processing Maps of 7005 Aluminum Alloy. *High Temp. Mater. Process.* **2014**, *33*, 369–375. [[CrossRef](#)]
44. Mondal, A.K.; Blawert, C.; Kumar, S. Corrosion Behaviour of Creep-Resistant AE42 Magnesium Alloy-Based Hybrid Composites Developed for Powertrain Applications. *Mater. Corros.* **2015**, *66*, 1150–1158. [[CrossRef](#)]
45. WANG, J.; SHI, B.; YANG, Y. Hot Compression Behavior and Processing Map of Cast Mg-4Al-2Sn-Y-Nd Alloy. *Trans. Nonferrous Met. Soc. China* **2014**, *24*, 626–631. [[CrossRef](#)]
46. Fan, Y.; Deng, K.; Wang, C.; Nie, K.; Shi, Q. Work Hardening and Softening Behavior of Mg–Zn–Ca Alloy Influenced by Deformable Ti Particles. *Mater. Sci. Eng. A* **2022**, *833*, 142336. [[CrossRef](#)]
47. Murashkin, M.; Sabirov, I.; Prosvirnin, D.; Ovid'ko, I.; Terentiev, V.; Valiev, R.; Dobatkin, S. Fatigue Behavior of an Ultrafine-Grained Al-Mg-Si Alloy Processed by High-Pressure Torsion. *Metals* **2015**, *5*, 578–590. [[CrossRef](#)]
48. Mokhtarishirazabad, M.; Azadi, M.; Hossein Farrahi, G.; Winter, G.; Eichlseder, W. Improvement of High Temperature Fatigue Lifetime in AZ91 Magnesium Alloy by Heat Treatment. *Mater. Sci. Eng. A* **2013**, *588*, 357–365. [[CrossRef](#)]
49. McCormigk, P.G. A Model for the Portevin-Le Chatelier Effect in Substitutional Alloys. *Acta Metall.* **1972**, *20*, 351–354. [[CrossRef](#)]
50. Yazdani, S.; Vitry, V. Using Molecular Dynamic Simulation to Understand the Deformation Mechanism in Cu, Ni, and Equimolar Cu-Ni Polycrystalline Alloys. *Alloys* **2023**, *2*, 77–88. [[CrossRef](#)]
51. Cottrell, A.H.; Dexter, D.L. Dislocations and Plastic Flow in Crystals. *Am. J. Phys.* **1954**, *22*, 242–243. [[CrossRef](#)]
52. LIU, M.; JIANG, T.; WANG, J.; LIU, Q.; WU, Z.; YU, Y.; SKARET, P.C.; ROVEN, H.J. Aging Behavior and Mechanical Properties of 6013 Aluminum Alloy Processed by Severe Plastic Deformation. *Trans. Nonferrous Met. Soc. China* **2014**, *24*, 3858–3865. [[CrossRef](#)]
53. Cuniberti, A.; Tolley, A.; Riglos, M.V.C.; Giovachini, R. Influence of Natural Aging on the Precipitation Hardening of an AlMgSi Alloy. *Mater. Sci. Eng. A* **2010**, *527*, 5307–5311. [[CrossRef](#)]
54. Yazdani, S.; Mesbah, M.; Vitry, V. Molecular Dynamics Simulation of the Interaction between Dislocations and Iron–Vanadium Precipitates in Alpha Iron: Effect of Chemical Composition. *Crystals* **2023**, *13*, 1247. [[CrossRef](#)]
55. Wang, W.H.; Wu, D.; Chen, R.S.; Zhang, X.N. Effect of Solute Atom Concentration and Precipitates on Serrated Flow in Mg-3Nd-Zn Alloy. *J. Mater. Sci. Technol.* **2018**, *34*, 1236–1242. [[CrossRef](#)]
56. Daroonparvar, M.; Khan, M.U.F.; Saadeh, Y.; Kay, C.M.; Kasar, A.K.; Kumar, P.; Esteves, L.; Misra, M.; Menezes, P.; Kalvala, P.R.; et al. Modification of Surface Hardness, Wear Resistance and Corrosion Resistance of Cold Spray Al Coated AZ31B Mg Alloy Using Cold Spray Double Layered Ta/Ti Coating in 3.5 wt % NaCl Solution. *Corros. Sci.* **2020**, *176*, 109029. [[CrossRef](#)]
57. Kim, H.-K.; Lee, Y.-I.; Chung, C.-S. Fatigue Properties of a Fine-Grained Magnesium Alloy Produced by Equal Channel Angular Pressing. *Scr. Mater.* **2005**, *52*, 473–477. [[CrossRef](#)]
58. CANDAN, S.; CANDAN, E. Comparative Study on Corrosion Behaviors of Mg-Al-Zn Alloys. *Trans. Nonferrous Met. Soc. China* **2018**, *28*, 642–650. [[CrossRef](#)]

59. Cheng, K.; Sun, J.; Xu, H.; Wang, J.; Zhou, J.; Tang, S.; Wang, X.; Zhang, L.; Du, Y. On the Temperature-Dependent Diffusion Growth of  $\phi$ -Mg<sub>5</sub>Al<sub>2</sub>Zn<sub>2</sub> Ternary Intermetallic Compound in the Mg-Al-Zn System. *J. Mater. Sci.* **2021**, *56*, 3488–3497. [[CrossRef](#)]
60. Alam, M.E.; Hamouda, A.M.S.; Nguyen, Q.B.; Gupta, M. Improving Microstructural and Mechanical Response of New AZ41 and AZ51 Magnesium Alloys through Simultaneous Addition of Nano-Sized Al<sub>2</sub>O<sub>3</sub> Particulates and Ca. *J. Alloys Compd.* **2013**, *574*, 565–572. [[CrossRef](#)]
61. Zhang, G.D.; Chen, R. Effect of the Interfacial Bonding Strength on the Mechanical Properties of Metal Matrix Composites. *Compos. Interfaces* **1993**, *1*, 337–355. [[CrossRef](#)]
62. Su, X.F.; Chen, H.R.; Kennedy, D.; Williams, F.W. Effects of Interphase Strength on the Damage Modes and Mechanical Behaviour of Metal–Matrix Composites. *Compos. Part A Appl. Sci. Manuf.* **1999**, *30*, 257–266. [[CrossRef](#)]
63. Vidal-Sétif, M.H.; Lancin, M.; Marhic, C.; Valle, R.; Raviart, J.-L.; Daux, J.-C.; Rabinovitch, M. On the Role of Brittle Interfacial Phases on the Mechanical Properties of Carbon Fibre Reinforced Al-Based Matrix Composites. *Mater. Sci. Eng. A* **1999**, *272*, 321–333. [[CrossRef](#)]
64. Wang, X.; Jiang, D.; Wu, G.; Li, B.; Li, P. Effect of Mg Content on the Mechanical Properties and Microstructure of Grf/Al Composite. *Mater. Sci. Eng. A* **2008**, *497*, 31–36. [[CrossRef](#)]

**Disclaimer/Publisher’s Note:** The statements, opinions and data contained in all publications are solely those of the individual author(s) and contributor(s) and not of MDPI and/or the editor(s). MDPI and/or the editor(s) disclaim responsibility for any injury to people or property resulting from any ideas, methods, instructions or products referred to in the content.